Soft Matter

Dynamic Article Links

Cite this: *Soft Matter*, 2012, **8**, 10008

www.rsc.org/softmatter

PAPER

Effect of confinement on molecular processes in the liquid crystal 8OCB: application of NMR relaxometry

M. Rajeswari,*[a] S. Dhara,[a] K. Venu,[b] V. S. S. Sastry[a] and R. Dabrowski[c]

Received 20th March 2012, Accepted 14th June 2012
DOI: 10.1039/c2sm25643f

Dispersions of proton spin–lattice relaxation rates (R_1) in the nematic and smectic phases of the liquid crystal 4′-octyloxy-4-cyanobiphenyl (8OCB), embedded in a nano-porous medium formed by an aerosil matrix, are investigated over a wide frequency (ν) range (10^4 Hz to 5×10^7 Hz) at two average pore sizes. In the low frequency (sub-MHz) region we observe a significant increase of R_1 in the confined samples, mediated by slow translational displacements (RMTD), arising from the formation of adsorption layers near the porous surface. Dispersion in this region is well accounted for by a power law behaviour ($R_1 \sim \omega^{-p}$), bracketed by low and high cutoff frequencies reflecting the limiting length scales of such displacements in these layers. The exponent p increases from 0.45 to 0.6 with a decrease of the temperature within the nematic phase, due to the progressive onset of longer wavelength diffusive modes within these layers. This signifies the onset of order director fluctuation (ODF) modes within the adsorption layers. Confinement is also seen to place restrictions on the long wavelength ODF modes of the bulk-like region of the liquid crystal, thus weakening considerably their dispersive effects in the low frequency region, relative to the bulk samples. In the smectic phase, p decreases appreciably signalling a depletion of such long range cooperative modes on layer formation. Analysis of the R_1 data also shows that individual dynamic processes like translational diffusion and reorientations of the molecules within the voids are largely unaffected due to confinement.

1 Introduction

The importance of the effects of quenched random disorder on the properties of liquid crystals (LCs) has been recognized previously,[1] and curious disorder-induced phenomena were experimentally investigated through, for example, calorimetry,[2] X-ray scattering and intensity fluctuations,[2,3] dielectric spectroscopy,[4–7] Fourier-transform infrared spectroscopy,[8] proton and deuteron nuclear magnetic resonance (DNMR)[9–12] and optical anisotropy measurements.[13] In this context, LC–aerosil systems were found to be particularly interesting because the random disorder could be introduced in a controlled manner unlike the cases with other random porous matrices like aerogels,[14] CPG[15–17] and anopore[18] *etc.* These nano sized particles embedded in the LC system on one hand provide an ordering mechanism even in the isotropic phase through surface interactions, and on the other tend to interfere with the long range orientational order of the mesophases, due to the finite sizes of the confining geometry.

Typically, the surface of the treated aerosil particles is covered with hydroxyl groups that tend to form hydrogen bonds with each other. At low densities ρ_s (<0.01 g cm^{-3}), the number of particles is too small to form a network and they act as impurities added to the LC. As the concentration increases above the gelation threshold, with ρ_s ranging from 0.01 to 0.1 (the relevant units are implied hereafter), the silica spheres are able to form a 3-D network, referred to as soft gel, and beyond this concentration, the network becomes more rigid, forming a stiff gel. The earlier proton NMR measurements in such confined LC systems (octylcyanobiphenyl (8CB) and octyloxycyanobiphenyl (8OCB)) were carried out in the isotropic phase.[9,10] In the present work, we extend these studies to mesophases in confined environments, focusing on the possible changes in the orientational structure factors, as effectively sensed by the diffusing LC molecules on cooling due to the progressive enhancement of ordering in the system. This problem was addressed earlier in 8CB–aerosil mixtures based on DNMR experiments,[11,12] and on calorimetric studies.[19,20]

Here we report on our proton spin–lattice relaxation rate (R_1) measurements of 8OCB in its nematic and smectic phases, both in the bulk state as well as under confinement by random networks of the aerosil particles, at two different concentrations.

[a]*School of Physics, University of Hyderabad, Hyderabad 500 046, India. E-mail: raji.hcu@gmail.com; Fax: +91-40-23010227; Tel: +91-40-23134318*
[b]*Soctronics Technologies Pvt. Ltd, Banjara Hills, Hyderabad 500 034, India*
[c]*Institute of Chemistry, Military University of Technology, Warsaw 00-908, Poland*

The frequency dispersion of R_1 is a measure of the cumulative power spectrum arising from the time modulation of the dominant spin–spin interactions effected by a variety of molecular processes. The confinement such as discussed above is known to introduce slow processes in the LC system near the porous surfaces, taking place typically in a low frequency regime (~kHz). For this purpose, we extend the dynamic range of the R_1 measurements to encompass slow time scales by adopting a recent technique based on the fast field cycling NMR (FFCNMR) principle.[21,22] This interesting method has proved to be particularly useful to study ultra slow processes in many soft materials, like polymers, protein dynamics, macromolecular processes, confined fluids, *etc.*[21] Dielectric measurements also give complementary information on molecular reorientational processes in liquid crystals and the earlier investigations on cyanobiphenyls with a wide range of aerosil concentrations confirm the presence of slow relaxation processes in confined systems and their temperature dependence shows a behavior typical for glass-forming liquids.[6,7]

The present paper is organized as follows. Experimental details related to the sample preparation and NMR measurements are given in Section 2. Relaxation mechanisms interpreting the experimental observations are discussed in Section 3, while a quantitative analysis of the data in terms of bulk and surface-induced relaxation mechanisms is presented in Section 4. The conclusions are summarized in the last Section.

2 Experimental details

The liquid crystal 8OCB, synthesized in our laboratory (Warsaw), has the phase sequence: I 353K N 340K SmA 327.5K Cr. The LC–aerosil mixtures were prepared using the solvent method.[2] Aerosil A300 consists of small silica spheres of diameter 7 nm and specific surface area 300 $m^2\ g^{-1}$. The small angle x-ray scattering (SAXS) investigation by Iannacchione *et al.* on these particles gives a hierarchical structure of different length scales. Their results suggested that the individual 7 nm particles fuse together during the manufacturing process to form a larger primary particle of size 21 nm. At higher concentrations these primary particles form aggregates of size 440 nm and these aggregates form further agglomerates.[2] These silica spheres were dried under vacuum at 473 K for over 15 hours, before being added to the LC diluted with pure acetone. The mixture was sonicated for about 2 hours to achieve a homogeneous dispersion and the solvent was then slowly evaporated over a long time (~10 hours) at 333 K. The surfaces of the spheres are covered with hydroxyl groups and interactions among them lead to a 3-D network within the LC medium. Because of the hydrophilic nature of the aerosil particles, the polar 8OCB molecules orient homeotropically at the surface. The densities of silica (ρ_s) in our two samples were 0.05 and 0.07 g cm^{-3}. The average void sizes formed by these networks were estimated to be 133 nm and 90 nm, respectively.[17] The shifts in the transition temperature due to the addition of these particles were within ±1 K.

Proton spin–lattice relaxation rates (R_1) were measured at different Larmor frequencies ranging from 10 kHz to 10 MHz using the field-cycling NMR Relaxometer (FCNMR, Stelar Spinmaster FFC 2000) and with a home-built pulsed field-variable spectrometer covering 10 MHz to 50 MHz. Pre-polarized and non-polarized pulse sequences were used[21,22] to measure R_1 on the FCNMR instrument, while an inversion recovery sequence was used at higher frequencies. The decay of magnetization was found to be exponential in all the experiments requiring a single relaxation time constant. Relative errors in the R_1 measurements were within 3% and the temperature of the sample was controlled to within ±0.1 K.

Fig. 1 shows the frequency dependence of the relaxation rates in bulk and confined LC samples in different mesophases, and the differences in the bulk profiles at different temperatures indicate very different underlying slow molecular processes

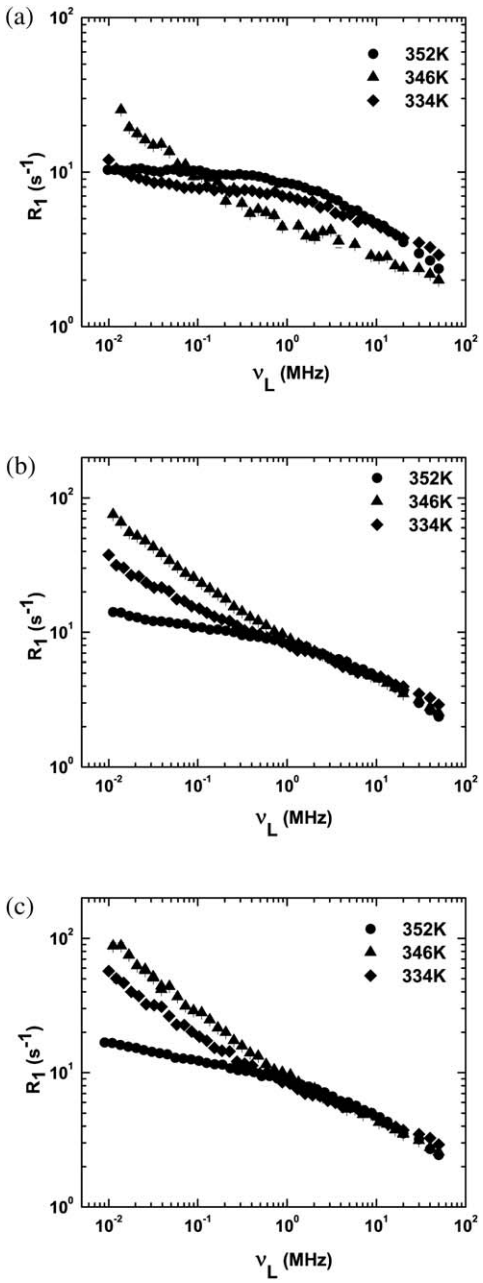

Fig. 1 The frequency dependence of the proton spin–lattice relaxation rate R_1 for 8OCB in the bulk (a), 8OCB + aerosil, at $\rho_s = 0.05$ (b), and 8OCB + aerosil, at $\rho_s = 0.07$ (c), at three temperatures: 352 K (just below the clearing temperature), 346 K (deep in the nematic phase), and 334 K (in the smectic phase).

effective at low frequencies. Progressive confinement with the two porous structures is seen to modify the bulk behaviour qualitatively. Fig. 2 exhibits the temperature dependence of these rates at different Larmor frequencies, bringing out contrasting features of the different phases in the bulk as well as in the confined systems.

3 Relaxation mechanisms

The spin–lattice relaxation of protons in these systems is predominantly mediated by the time modulation of dipole–dipole interactions between the spins, caused by processes such as molecular reorientations, translational diffusion and collective modes like order parameter fluctuations (OPF), order director fluctuations (ODF) or layer undulations (LU). Significant interactions of the LC molecules with the confining surfaces could lead to surface diffusion modes with constrained molecular orientations, leading to slow processes relevant to the present experiment. The molecular dynamic models of interest to our study are briefly presented here.[23–26]

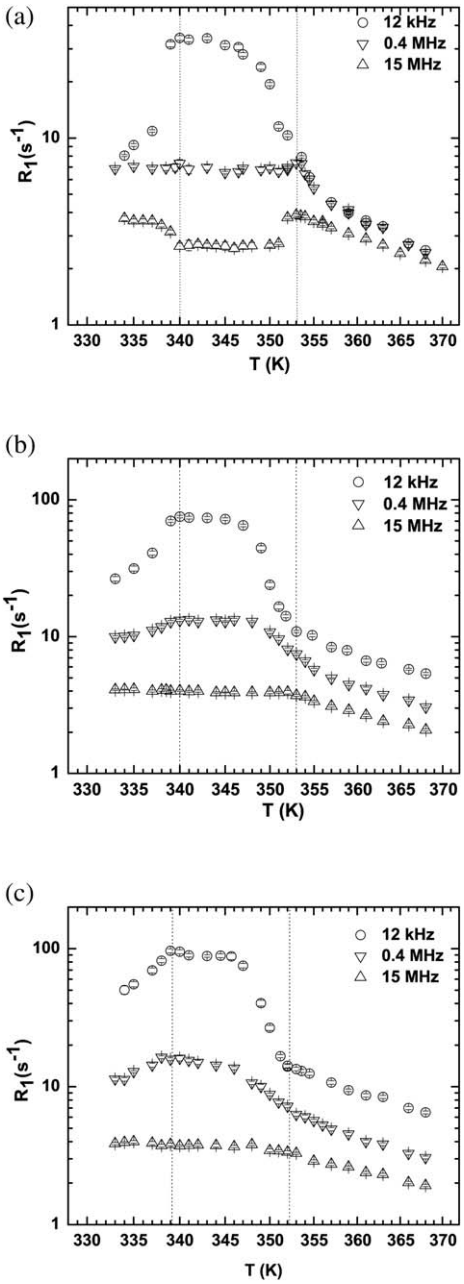

Fig. 2 The temperature dependence of the proton spin–lattice relaxation rate R_1 at three Larmor frequencies for 8OCB in the bulk (a), 8OCB + aerosil, at $\rho_s = 0.05$ (b), and 8OCB + aerosil, at $\rho_s = 0.07$ (c). The phase transition temperatures are indicated by vertical dotted lines.

3.1 Rotational dynamics (R)

Molecular reorientations and conformational changes modulate the dipolar interaction, providing a relaxation pathway. However within the frequency range of the experiment limited by the largest Larmor frequency, all processes faster than $\sim 10^{-9}$ are white-noise like, and do not contribute to observable dispersion. Only reorientations about the short axes of the molecules (R) typically lead to slight dispersion at the high frequency end. This contribution is well-accounted for by the BPP theory,[24,27] as

$$R_{1R} = A_R \sum_{p=1}^{2} \frac{p^2 \tau_R}{1 + (p\omega\tau_R)^2}. \quad (1)$$

Here A_R quantifies the contribution from the reorientations.

3.2 Molecular translational self-diffusion (SD)

Intermolecular spin interactions are modulated by (random) molecular translational displacements. Their contribution to the relaxation rate (R_{1SD}) was calculated analytically for viscous isotropic liquids,[28] and was subsequently extended to the nematic and smectic A phases.[29,30] Its contribution was shown to be effectively given by

$$R_{1SD} = \frac{1}{1.4}(R_1)_{\text{Torrey}}. \quad (2)$$

This model in turn implies[28] specification of the (average) diffusion constant D and the coupling strength A_D of the spins to the lattice modes through this mechanism.

3.3 Order parameter fluctuations (OPF)

At the onset of the nematic phase, *i.e.*, just below the isotropic–nematic transition temperature T_{NI}, fluctuations in the magnitude of the nematic order parameter S are effective in relaxing the nuclear spins, *i.e.* the fluctuations in the long-range orientational order modulates the dipole–dipole interactions between the nuclear spins providing additional mechanisms for spin–lattice relaxation. Within the small temperature region where these order parameter fluctuations (OPF) are dominant (typically within a few degrees below the clearing point), these processes contribute appreciably to the relaxation rate through their spectral density given by[23]

$$J(m_L\omega) = A_{OPF}\left[\frac{\tau_{OPF}}{1 + \sqrt{1 + (m_L\omega\tau_{OPF})^2}}\right]^{\frac{1}{2}} \quad (m_L = 1, 2). \quad (3)$$

Here τ_{OPF} is the characteristic time associated with the fluctuation of the long-range order, and A_{OPF} is a measure of the lattice coupling that this mechanism provides to the spin system.

3.4 Order director fluctuations (ODF)

Order director fluctuations are characteristic collective (hydrodynamic) modes in the nematic phase, and provide distinct slow modulations of spin interactions. Their wave-vector dependent life times in principle relate to the three elastic distortions (splay, twist and bend with constants K_1, K_2, and K_3, respectively), and associated viscosities.[31] Under the assumption of equal values for these constants (one constant approximation, *i.e.* $K_1 = K_2 = K_3 = K$), a simplified expression for the spectral density of the fluctuations arising from these processes results as an integral over an interval of wave vectors defined by the limiting scales in the system[23]

$$J_1(\omega)_{\mathrm{ODF}} = \frac{V}{(2\pi)^3}\int_{q_{\min}}^{q_{\max}} \frac{k_{\mathrm{B}}T}{VKq^2} \times \frac{\tau(q)}{1+\omega^2\tau^2(q)} 4\pi q^2 \mathrm{d}q.$$

Here $q_{\min}$ and $q_{\max}$ are determined by the largest and smallest sustainable wavelengths dictated by the visco-elastic characteristics of the LC phase and the geometry of the sample. These are translated as the corresponding limiting frequencies ω_{ODFmin} and ω_{ODFmax} of the dispersion profile ($\omega = Kq^2/\eta$). For small enough amplitudes of these fluctuations, the corresponding contribution to R_1 is expressed as[23]

$$R_{1\mathrm{ODF}} = \frac{A_{\mathrm{ODF}}}{\omega^{1/2}}\left[f\left(\frac{\omega_{\mathrm{ODFmax}}}{\omega}\right) - f\left(\frac{\omega_{\mathrm{ODFmin}}}{\omega}\right)\right] \quad (4)$$

where

$$f(y) = \frac{1}{\pi}\left[\arctan\left(\sqrt{2y}+1\right) + \arctan\left(\sqrt{2y}-1\right) - \arctan\left(\frac{\sqrt{2y}}{y+1}\right)\right]. \quad (5)$$

Here A_{ODF} depends upon, amongst others, the degree of the orientational order ($\sim S^2$), and provides a measure of the efficacy of the ODF mechanism in mediating the spin–lattice relaxation.

3.5 Layer undulations (LU)

At the onset of the smectic A phase, layer undulations provide another class of slow modulations, arising from the splay deformations sustained over long length scales. The twist and bend distortions are not energetically feasible in the layered structures and hence are expelled. The corresponding relaxation rate is given by[23]

$$R_{1\mathrm{LU}} = \frac{A_{\mathrm{LU}}}{\omega\pi}\left[\arctan\left(\frac{\omega_{\mathrm{LU\,max}}}{\omega}\right) - \arctan\left(\frac{\omega_{\mathrm{LU\,min}}}{\omega}\right)\right]. \quad (6)$$

Here A_{LU} measures the strength of this mechanism. ω_{LUmax} and ω_{LUmin} provide the two bracketing high and low frequency cutoff values for this dispersion, arising from considerations similar to the ODF modes.

3.6 Reorientations mediated by translational displacements (RMTD)

The enhancement of the relaxation rates observed in the confined samples in the low frequency regime of the dispersion profiles (Fig. 1) is indicative of the onset of slow processes arising from the anchoring interaction between the LC molecules and the surface. Translational displacements in the presence of surface-induced ordering within the adsorption layer leads to relatively long correlation times among the (short-axes) molecular reorientations, and hence to significant additional contributions to the spectral densities at lower frequencies. The time scales of the RMTD mechanism are determined both by the translational mobility of the probe molecules specified by the diffusion coefficient D, as well as the relatively larger length scales of the roughness of the porous surface (compared to molecular displacements) quantified by the wave-vector dependent orientational surface structure factor. The corresponding orientational time correlation function of the probe molecule between the limits, say, $q_{\min}$ and $q_{\max}$ of the RMTD process, is expressed as[25]

$$G(t) = \int_{q_{\min}}^{q_{\max}} S(q)\mathrm{e}^{-Dtq^2}\mathrm{d}q.$$

Here $S(q)$ is the orientational structure factor. Thus the derived spectral density $J_k(\omega)_{\mathrm{RMTD}}$ contains Lorentzian-type contributions of all the q-modes, weighted by the orientational structure factor $S(q)$, and is written as

$$J_k(\omega)_{\mathrm{RMTD}} = \int_{q_{\min}}^{q_{\max}} S(q)\frac{2\tau_q}{1+\omega^2{\tau_q}^2}\,\mathrm{d}q$$

where

$$\tau_q = \frac{1}{Dq^2}.$$

Within the assumption of the isotropic distribution of pores in the random porous media,[26] $J_2(\omega)_{\mathrm{RMTD}} = 4J_1(\omega)_{\mathrm{RMTD}}$.

For a constant orientational structure factor, the corresponding relaxation rate induced by the RMTD process is expressed as[21,26,32]

$$R_{1\mathrm{RMTD}} = A_{\mathrm{RMTD}}\left\{\frac{1}{\omega^{1/2}}\left[f\left(\frac{\omega_{\mathrm{RMTD\,max}}}{\omega}\right) - f\left(\frac{\omega_{\mathrm{RMTD\,min}}}{\omega}\right)\right] + \frac{4}{(2\omega)^{1/2}}\left[f\left(\frac{\omega_{\mathrm{RMTD\,max}}}{2\omega}\right) - f\left(\frac{\omega_{\mathrm{RMTD\,min}}}{2\omega}\right)\right]\right\}, \quad (7)$$

where $f\left(\frac{\omega_{\mathrm{RMTD\,max}}}{\omega}\right)$ and $f\left(\frac{\omega_{\mathrm{RMTD\,min}}}{\omega}\right)$ are given by eqn (5). The prefactor A_{RMTD} depends on the diffusion coefficient, geometrical features of the confined matrix and residual dipole–dipole interactions among the proton spins. Such effects of the RMTD mechanism on the spin–lattice relaxation dispersion were observed previously in other porous systems like liquid crystals in random porous glass,[26,32] in polymers[21] and water as well as polar and non-polar liquids in different random porous matrices.[25,33,34] In real systems the surface structure factor is indeed dependent on the amplitude of the wave-vector (q), and the expression for relaxation rate needs to be derived suitably. For a specific q dependence, *viz* $S(q) = cq^{-\chi} + e$,[26] the relaxation rate assumes a simple and interesting frequency dependence with a power law dependence on q between its minimum and maximum realizable values ($R_{1\mathrm{RMTD}} \sim \omega^{-p}$).

4 Analysis and discussion

Analysis of the frequency dispersion of the spin–lattice relaxation rate (R_{1B}) of bulk liquid crystal just below T_{NI} requires the invoking of the following relaxation mechanisms: reorientations about the short axes (R), translational self-diffusion (SD) and order parameter fluctuations (OPF). In confined systems an additional mechanism arising from the RMTD dynamics also contributes to the corresponding total relaxation (R_{1C}). Thus these two total relaxation rates are expressed as

$$R_{1B} = R_{1R} + R_{1SD} + R_{1OPF} \quad (8)$$

$$R_{1C} = R_{1R} + R_{1SD} + R_{1OPF} + R_{1RMTD}. \quad (9)$$

The bulk liquid crystal dispersion data just below the clearing temperature at 352 K (*i.e.* $\Delta T_{NI} = T - T_{NI} = -1$ K), are analysed based on eqn (8) using the suitable non-linear least squares method[35] and the resulting fit is shown in Fig. 3a. The experimental value of the diffusion coefficient D[36,37] was used in our analysis, as an input parameter. The free parameters in the fitting procedure are thus the coupling constant associated with diffusion A_D, the coupling strength of the reorientations A_R, the reorientational correlation time around the short axes τ_R, and the prefactor A_{OPF} characterizing the contribution from order parameter fluctuations along with their correlation time τ_{OPF}. The results of the analysis are summarized in Table 1. We find that A_D decreases from 25 s^{-2} at 353.6 K (isotropic phase)[10] to 19.7 s^{-2} in the nematic phase, while A_R remains essentially the same (see Table 1). The slight change in the extracted reorientational correlation time τ_R from 7.6 to 8.2 ns on cooling across the transition is within the error of estimation. Major change however is seen in the time scale of the order parameter fluctuations τ_{OPF} from 183 ns in the isotropic phase at 353.6 K to 433 ns at 352 K, and in the A_{OPF} values as the nematic phase forms.[10]

The confined LC dispersion profiles at the two concentrations of the aerosil particles were analysed based on eqn (9), and the fits are shown in Fig. 3b and c. The confinement of the LC to the random porous matrix is seen clearly inducing slow dynamic components near the surface, originating from the relatively more persistent time correlations among the molecular reorientations brought about by molecular diffusion very near the locally ordering porous surface (RMTD). Comparing the values of the model parameters extracted in the bulk system at this temperature with the corresponding data of the confined systems (Table 1), we find that A_D decreases at both the concentrations. The observed decrease in the reorientational correlation time τ_R on the confinement from its bulk value, *i.e.* from 8 to 6 ns at $\rho_s = 0.05$ and to 5.4 ns at $\rho_s = 0.07$, seems to be a clear manifestation of the surface ordering on the local individual molecular processes. The exponent associated with the RMTD mechanism ($R_1 \sim \omega^{-p}$)[26] changes from 0.38 in the isotropic phase to 0.45 (± 0.05) just below the transition.[10] The so-called equipartition value of this exponent (0.5), which would have resulted by assuming an orientational structure factor with no wave-vector dependence, is comparable to the value just below the transition (0.45) within estimation error. The degree of the coupling of the spin system to the lattice *via* the RMTD mechanism A_{RMTD} also changes significantly across the transition.

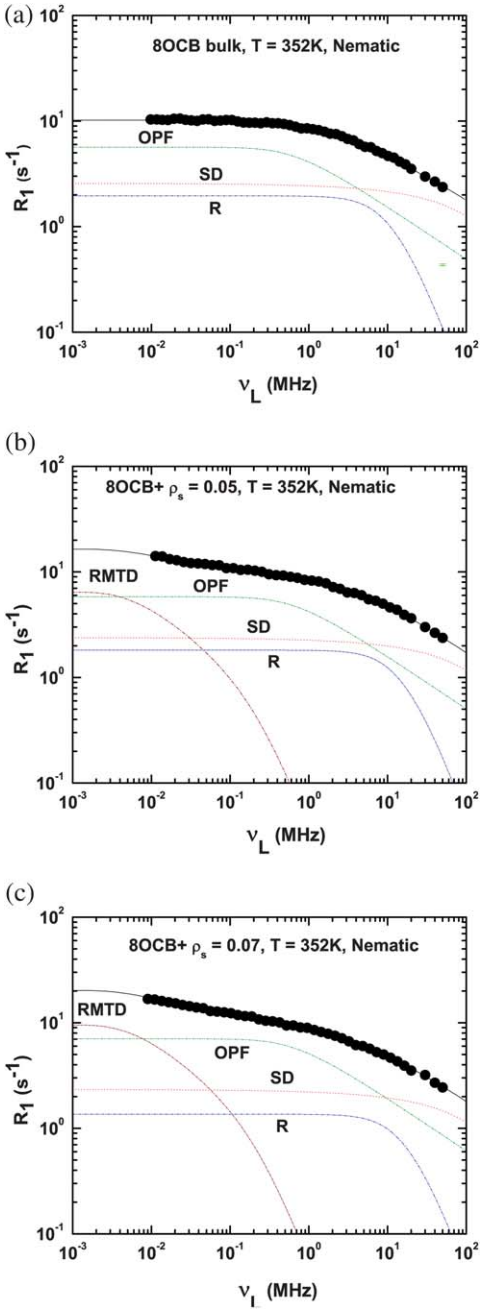

Fig. 3 Frequency dispersion of the proton spin–lattice relaxation rate of 8OCB at 352 K ($\Delta T_{NI} = -1$ K): (a) bulk, (b) 8OCB + aerosil, at $\rho_s = 0.05$, (c) and 8OCB + aerosil, at $\rho_s = 0.07$. The dotted color lines represent the contributions from the different molecular processes.

In the mid-nematic phase and just above the smectic–nematic phase transition temperature T_{AN} (at T = 346 and 341 K, respectively) the relaxation rates in the bulk sample (R_{1B}) profiles were analysed based on the following relevant mechanisms: molecular reorientations (R), translational diffusion (SD) and order director fluctuations (ODF). Those in confined LC profiles (R_{1C}) were analysed by including the additional RMTD mechanism. The corresponding relaxation rates in this temperature region are then expressed as

$$R_{1B} = R_{1R} + R_{1SD} + R_{1ODF} \quad (10)$$

Table 1 The best fit parameters obtained from the experimental data in the nematic and smectic phases, based on the contributions explained in Section 3

Sample	Pure 8OCB				8OCB + aerosil, $\rho_s = 0.05$				8OCB + aerosil, $\rho_s = 0.07$			
T (K)	352	346	341	334	352	346	341	334	352	346	341	334
$A_D\ 10^8\ s^{-2}$	19.73	9.42	8.55	1.33	18.27	13.0	10.85	1.41	17.88	13.86	10.59	1.27
$D\ 10^{-11}\ m^2\ s^{-1}$	9.8	7.5	6.3	0.36	9.8	7.5	6.3	0.36	9.8	7.5	6.3	0.36
$A_R\ 10^9\ s^{-2}$	0.24	1.5	1.5	4.46	0.3	1.5	1.5	4.32	0.25	1.5	1.5	4.26
$\tau_R\ 10^{-9}$ s	8.15	0.75	0.7	0.75	6.04	0.75	0.7	0.79	5.44	0.75	0.7	0.80
$A_{OPF}\ 10^3\ s^{-3/2}$	12.31	—	—	—	12.65	—	—	—	15.33	—	—	—
$\tau_{OPF}\ 10^{-9}$ s	422.9	—	—	—	422.9	—	—	—	422.9	—	—	—
$A_{ODF}\ 10^3\ s^{-3/2}$	—	5.84	7.2		—	5.84	7.2		—	5.84	7.2	
$\omega_{ODFmin}/2\pi$ kHz	—	1	1		—	4.7×10^3	6.7×10^3		—	5.9×10^3	7×10^3	
$\omega_{ODFmax}/2\pi$ MHz	—	100	100		—	100	100		—	100	100	
$A_{LU}\ 10^3 s^{-3/2}$	—	—	—	395.9	—	—	—	395.9	—	—	—	395.9
$\omega_{LU\ min}/2\pi$ kHz	—	—	—	0.1	—	—	—	0.1	—	—	—	0.1
$\omega_{LUmax}/2\pi$ MHz	—	—	—	100	—	—	—	100	—	—	—	100
$A_{RMTD}\ 10^2 s^{-(1+p)}$	—	—	—	—	2.08	88.8	93.8	17.9	3.07	161.58	204.71	49.9
$\omega_{RMTDmin}/2\pi$ kHz	—	—	—	—	6.5	1	1	0.1	6.5	1	1	0.1
$\omega_{RMTDmax}/2\pi$ MHz	—	—	—	—	0.5	150	50.5	3.5	0.5	65.1	46.2	3.5
p	—	—	—	—	0.45	0.55	0.55	0.50	0.45	0.58	0.59	0.54

$$R_{1C} = R_{1R} + R_{1SD} + R_{1ODF} + R_{1RMTD}. \quad (11)$$

The results of the analysis of the bulk data (eqn (10)) are depicted in Fig. 4. The data show a power law behavior of the relaxation rate ($R_1 \sim \omega^{-1/2}$) arising from the classical ODF mechanism (within the single elastic constant approximation and the assumption of the wave-vector independent viscosities), between two cutoff frequencies. The lower cutoff frequency in effect marks the upper bound of the long wavelength ODF modes sustained in the nematic medium, and the ODF contribution below this cutoff frequency levels off leading a plateau in the dispersion profile. But such an observation may not be always accessible in the FCNMR experiment due to its inherent limitations. The interpretation of the observed magnetization recovery in terms of the well defined spin–lattice relaxation time constant T_1 is constrained in a field-cycling experiment at very low Zeeman fields due to the presence of comparable local fields. This requirement on the lowest accessible Zeeman field (to be higher than typical dipolar fields) thus restricts the profile to about $\sim 10^4$ Hz. The absence of a cutoff in the experimental data (Fig. 4) is understood in this context, and the value used in the fitting procedure is only indicative that such a frequency is well below the lowest accessible frequency of the experiment. The higher cutoff frequency in these systems falls typically well above the highest frequency of such experiments, and the value was hence fixed at 100 MHz as is the case in such experiments.[26] Thus the ODF contribution to the bulk data in the mid-nematic region has the typical $\omega^{-1/2}$-type dependence of the relaxation rate over the entire frequency region covered by the present experiment, practically unhindered by the limitations on the lower and upper wavelengths of these modes.

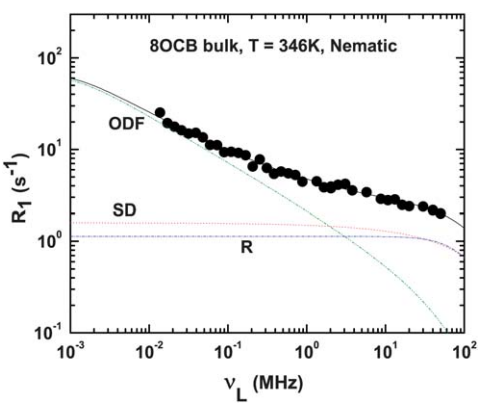

Fig. 4 Frequency dispersion of the proton spin–lattice relaxation rate of the bulk 8OCB at $T = 346$ K. The dotted color lines represent the contributions from the different molecular processes.

Analysis of the confined system, based on eqn (11), was carried out utilizing the model parameters extracted from the bulk data as useful inputs. An interesting aspect of this profile is that there could in principle be power law type contributions ($R_1 \sim \omega^{-p}$) to the dispersion profile both from the ODF mechanism as well as from the RMTD process. To resolve this issue, we first analysed this data with a simple power law, say $(R_1)_x \sim \omega^{-p}$, without assigning a specific underlying mechanism, bracketed of course by the two limiting frequencies. The exponent p for this fit was found to be 0.52 and 0.56 at 346 K at the two concentrations, respectively (Fig. 5). This exponent could in principle be assigned entirely as being due to the ODF mechanism, and viewed as a consequence of an increase in the relaxation rate upon confinement, arising from the fractal nature of the director fluctuations in the cavities, as suggested by Leon *et al.*[38] However counter arguments against this interpretation,[26] based on the consequence of fractional dimensionality on the calculation of the associated length scales which then would tend to be unrealistic, favour our interpretation of the confined data both in terms of (the known) ODF and confinement-induced RMTD process. Thus, we preferred to analyse the data with the additional RMTD mechanism along with the ODF mechanism (details of which are already known from the bulk data), while fully recognizing their competing nature in the mid-frequency region (above ω_{ODFmin}). However, under these circumstances specific assignment of the relative contributions of the two processes cannot be said to be unique. Frequency dispersion of the relaxation rate below ω_{ODFmin}, if any, can however be reasonably attributed to the RMTD process, and the corresponding

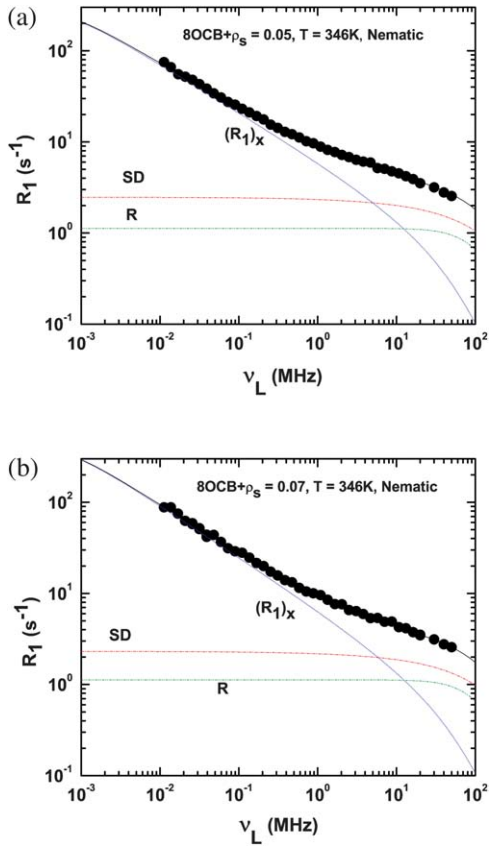

Fig. 5 Frequency dispersion of the proton spin–lattice relaxation rate at $T = 346$ K: (a) 8OCB + aerosil, at $\rho_s = 0.05$, (b) 8OCB + aerosil, at $\rho_s = 0.07$. The color dotted lines are the contributions from the different molecular processes.

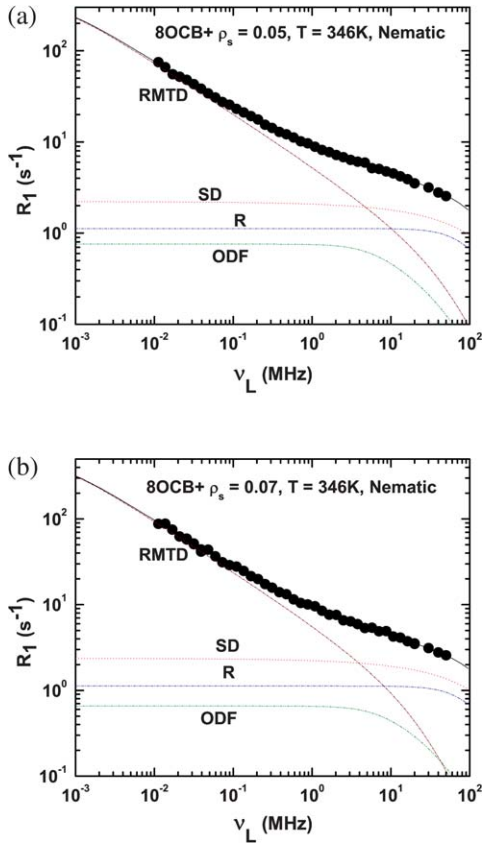

Fig. 6 Frequency dispersion of the proton spin–lattice relaxation rate of 8OCB at 346 K: (a) 8OCB + aerosil, at $\rho_s = 0.05$, (b) and 8OCB + aerosil, at $\rho_s = 0.07$. The color dotted lines are the contributions from the different molecular processes.

parameters could be usefully considered with some confidence for appreciating the effects of the surface interactions. With this caveat, we analysed the low-frequency data in terms of $R_{1\mathrm{ODF}} + R_{1\mathrm{RMTD}}$, obtaining quantitative contributions from both the ODF and RMTD processes. For this purpose, the low frequency cutoff of ODF is left as a free parameter and A_{ODF} is fixed at the bulk value. The results of these fits at 346 K are shown in Fig. 6, and the fitted parameters at all temperatures are shown in Table 1. The lower cutoff frequencies of the ODF mechanism in the confined samples are now found to have shifted to much higher frequencies relative to the bulk values (~kHz), and are 4.7 MHz for $\rho_s = 0.05$ and 5.9 MHz for $\rho_s = 0.07$, at 346 K. Their values further increase with the decrease of temperature in the nematic phase. This increasing restriction on the upper bound of the long wavelength ODF modes (on cooling) seems to be a direct consequence of the confinement on the ODF process in the bulk region of the confined sample. This also has the welcome consequence of allowing the observed dispersion below this cut-off value to be interpreted as essentially due to the RMTD, facilitating its quantitative analysis.

The fits shown in Fig. 6 clearly bring out the importance of the RMTD mechanism at low frequencies, with exponent values 0.55 ± 0.007 and 0.58 ± 0.01. The increase in the exponent associated with this mechanism, from 0.45 near the transition to 0.55 in the mid-nematic phase, is interesting evidence of the onset of the longer wavelength ODF modes within the adsorption layers imparting relatively more significant weight to these length scales in the surface orientational structure factor. The exponent value also shows a marginal increase with the concentration of aerosil particles, hinting at its, though weaker, dependence on the void/pore size. Also, the RMTD interaction strength A_{RMTD} was found to increase by an order of magnitude in the nematic phase. Further, the decrease of the higher frequency cutoff value of the ω_{RMTD} with the decrease of temperature is a pointer to the enhancement of the surface-induced order in the voids. The lower cutoff frequency for RMTD could not be estimated since the data did not taper off to a low frequency plateau within the experimental range. Thus the effect of the confinement on a nematic system with fairly well-developed orientational order could be inferred by both the ODF effects on the bulk-like region of the sample, as well as by the modified orientational structure factor of the porous surfaces as reported by the RMTD contribution.

The best-fit low frequency cutoff values of the collective processes such as the RMTD and ODF mechanisms are related to the largest diffusion time of RMTD during which the orientational correlation is lost $\tau_{\mathrm{RMTDmax}} = (\omega_{\mathrm{RMTDmin}})^{-1}$ and the decay time of the slowest director fluctuations, $\tau_{\mathrm{ODFmax}} = (\omega_{\mathrm{ODFmin}})^{-1}$. These values at 346 K are found to be 16×10^{-5} and 27×10^{-9} s. The decay time of the director fluctuations are

shorter by four orders of magnitude than the RMTD process and this clearly suggests that these two mechanism are distinctly separable in the frequency range of our study. The maximum distance that a molecule could travel in the voids is estimated as $l_{\mathrm{RMTD\,max}} = \sqrt{2D_{\parallel}(\tau_{\mathrm{RMTD\,max}})} = 154$ nm and the maximum wavelength of the director fluctuations is calculated to be $\lambda_{\mathrm{ODF\,max}} = \sqrt{4\pi^2 K/\eta\omega_{\mathrm{ODF\,min}}} \sim 20$ nm. This shows that the spatial confinement imposes restrictions on the ODF modes. The length and time scales of the collective processes further indicate strong surface anchoring of the LC in the aerosil matrix.

In the smectic phase of the bulk system, the high frequency dispersion is usually expected from reorientations and self-diffusion process, while the low frequency dispersion is expected primarily from the slow layer undulations (LU).[23] The ODF process is not expected to be as significant as in the nematic phase on general arguments: the bend and twist distortions are known to be energetically costly on layer formation and hence their contribution to the ODF dynamics should be decreased significantly. It is then reasonable to attempt to fit the bulk data with only the R, SD and LU mechanisms.[39,40] Thus we write the total relaxation rate in the bulk smectic phase at $T = 334$ K ($R_{1\mathrm{B}}$) as,

$$R_{1\mathrm{B}} = R_{1\mathrm{R}} + R_{1\mathrm{SD}} + R_{1\mathrm{LU}}. \quad (12)$$

For the confined smectic system, we introduce the additional RMTD mechanism to account for the observed enhancement on the confinement, and write the corresponding relaxation rate $R_{1\mathrm{C}}$ as,

$$R_{1\mathrm{C}} = R_{1\mathrm{R}} + R_{1\mathrm{SD}} + R_{1\mathrm{LU}} + R_{1\mathrm{RMTD}}. \quad (13)$$

Analysis of the bulk smectic data (eqn (12)) leads to the assignment of the relative contributions as shown in Fig. 7a. It appears that the layer undulations are very effective below 100 kHz, while the SD is generally dominant in the sub-MHz regime. Individual molecular reorientations are effective at higher frequencies as expected. Fig. 7b and c show the results of the analysis of the confined smectic phase data based on eqn (13). We immediately observe that it is not possible to uniquely distinguish between the contributions of LU and RMTD mechanisms at low frequencies as they compete in the same frequency regime, unlike the case of the ODF mechanism in the nematic phase. The exponent value of RMTD marginally decreases to 0.53 and below, depending on the aerosil density, indicating the somewhat lowered importance of the longer wavelength diffusion modes to the RMTD at the onset of the smectic phase. These findings are interesting, particularly in contrast with similar relaxometric results on another related LC (octylcyanobiphenyl—8CB), confined to random porous glass (CPG of diameter 15 nm). In the latter system there was no specific signature of the onset of the smectic phase, nor evidence of the diminished role of the long wavelength diffusive modes on the surface. In fact the corresponding exponent was reported to increase continually as one cools the system in the smectic phase.[26]

Thus, the present system confined to a 3-D porous structure with comparable lateral dimensions in all directions seems to be sensitive to the onset of layer formation, as evidenced by the changes in the data across the N–Sm A transition. For example, Fig. 2 shows (say, data at 12 kHz in these figures across the N–Sm A transition) that the onset of the smectic phase leads to a discernible decrease of the relaxation rate corresponding to low frequency modes, both in the bulk as well as in confined systems. This loss becomes progressively smaller with enhanced confinement. This is to be compared with results reported earlier across the same transition in 8CB but with a cylindrical confinement (CPG) under much more severe geometric restrictions.[26] It appears that this transition was wiped out in the previous case due to a high degree of confinement, while the present work could bring out the effect of such a layering transition on the dynamics of the confined system. We conclude that within the limits to which we could restrict the system in our experiments, the smectic phase is effectively inhibiting the long wavelength modes, resulting in a corresponding decrease in the exponent of the RMTD.

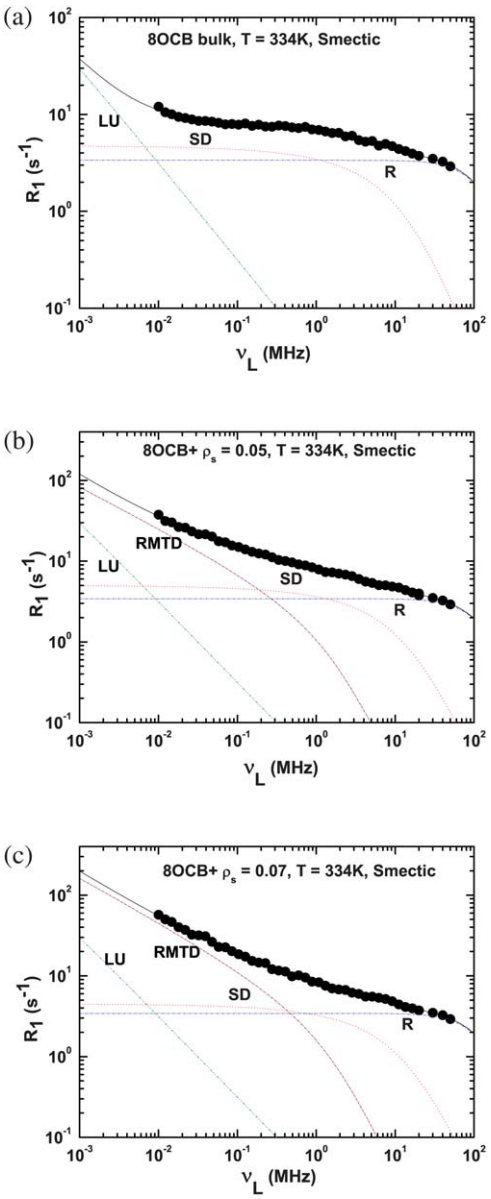

Fig. 7 Frequency dispersion of the proton spin–lattice relaxation rate of 8OCB at 334 K: (a) bulk, (b) 8OCB + aerosil, at $\rho_s = 0.05$, and (c) 8OCB + aerosil, at $\rho_s = 0.07$. The color dotted lines are the contributions from the different molecular processes.

5 Conclusions

We measured the frequency dispersion of proton spin–lattice relaxation rates of 8OCB in bulk form and in two samples embedded in random porous 3-D networks formed by aerosil nano-particles, at two different average pore sizes. The observed increase in the relaxation rate in the low frequency regime is interpreted as due to the slow reorientational correlations of the LC molecules undergoing diffusion processes within the adsorption layers near the porous surfaces. We find that as the thermodynamic phase of the LC medium undergoes progressive changes with a decrease in temperature, the characteristics of the slow dynamics also correspondingly change. These are reflected in two ways: the change in the power law behaviour of the relaxation rate between the two cutoff frequency limits of the RMTD process, and the efficacy of the RMTD mechanism in contributing to R_1. The variation of this power law exponent, for a given topology of the embedding network, is thus an indication of the subtle changes in the characteristics of the adsorption layer induced by changes in the ordering of the LC medium on cooling. We find that this exponent increases from 0.45 to 0.6 as the confined system is cooled in its nematic range. This is interpreted as a progressive onset of order director fluctuations within these adsorption layers, promoting correlated nematic regions over longer length scales, consistent with the behaviour of the central core region. This is further supported by a corresponding increase (by an order of magnitude) in the coupling strength of the spin–lattice relaxation to the RMTD mechanism. The onset of the smectic phase dramatically changes this exponent value from 0.6 to 0.5, interpreted as due to the relative losses of the contribution from the long wavelength modes on the formation of smectic layers, and results on the bulk sample in the corresponding phase also support this interesting scenario. We also report in this process dynamic parameters connected with individual processes (molecular reorientations and translational diffusion). This work also shows the sensitivity of a 3-D confined LC system to layer formation, in contrast to the system earlier investigated under severe CPG confinement.

References

1 G. P. Crawford and S. Zumer, *Liquid Crystals in Complex Geometries*, Taylor and Francis, London, 1996.
2 G. S. Iannacchione, C. W. Garland, J. T. Mang and T. P. Rieker, *Phys. Rev. E: Stat. Phys., Plasmas, Fluids, Relat. Interdiscip. Top.*, 1998, **58**, 5966–5981.
3 A. Roshi, S. Barjami, G. Iannacchione, D. Paterson and I. Mcnulty, *Phys. Rev. E: Stat., Nonlinear, Soft Matter Phys.*, 2006, **74**, 031404.
4 A. Hourri, T. K. Bose and J. Theon, *Phys. Rev. E: Stat., Nonlinear, Soft Matter Phys.*, 2001, **63**, 051702.
5 J. Leys, C. Glorieux and J. Theon, *J. Phys.: Condens. Matter*, 2008, **20**, 244111.
6 S. Frunza, L. Frunza, H. Goering, H. Sturm and A. Schonhals, *Europhys. Lett.*, 2001, **56**, 801–807.
7 S. Frunza, L. Frunza, M. Tintaru, I. Enache, T. Beica and A. Schonhals, *Liq. Cryst.*, 2004, **31**, 913–922.
8 M. Jasiurkowska, W. Kossack, R. Ene, C. Iacob, W. K. Kipnusu, P. Papadopoulos, J. R. Sangoro, M. Massalska-Arodz and F. Kremer, *Soft Matter*, 2012, **8**, 5194–5200.
9 E. Anoardo, F. Grinberg, M. Vilfan and R. Kimmich, *Chem. Phys.*, 2004, **297**, 99–110.
10 M. Rajeswari, S. Dhara, K. Venu, V. S. S. Sastry and R. Dabrowski, *Mol. Cryst. Liq. Cryst.*, 2011, **546**, 45–56.
11 T. Jin and D. Finotello, *Phys. Rev. Lett.*, 2001, **86**, 818–821.
12 T. Jin and D. Finotello, *Phys. Rev. E: Stat., Nonlinear, Soft Matter Phys.*, 2004, **69**, 041704.
13 T. Bellini, M. Buscaglia, C. Chiccoli, F. Mantegazza, P. Pasini and C. Zannoni, *Phys. Rev. Lett.*, 2000, **85**, 1008–1011.
14 N. A. Clark, T. Bellini, R. M. Malzbender, B. N. Thomas, A. G. Rappaport, C. D. Muzny, D. W. Schaefer and L. Hrubesh, *Phys. Rev. Lett.*, 1993, **71**, 3505–3508.
15 S. Kralj, A. Zidansek, G. Lahajnar, I. Musevic, S. Zumer, R. Blinc and M. M. Pintar, *Phys. Rev. E: Stat. Phys., Plasmas, Fluids, Relat. Interdiscip. Top.*, 1996, **53**, 3629–3638.
16 M. D. Dadmun and M. Muthukumar, *J. Chem. Phys.*, 1993, **98**, 4850–4852.
17 G. S. Iannacchione, *Fluid Phase Equilib.*, 2004, **222–223**, 177–187.
18 G. S. Iannacchione and D. Finotello, *Phys. Rev. Lett.*, 1992, **69**, 2094–2097.
19 P. S. Clegg, C. Stock, R. J. Birgeneau, C. W. Garland, A. Roshi and G. S. Iannacchione, *Phys. Rev. E: Stat., Nonlinear, Soft Matter Phys.*, 2003, **67**, 021703.
20 A. Roshi, G. S. Iannacchione, P. S. Clegg and R. J. Birgeneau, *Phys. Rev. E: Stat., Nonlinear, Soft Matter Phys.*, 2004, **69**, 031703.
21 R. Kimmich and E. Anoardo, *Prog. Nucl. Magn. Reson. Spectrosc.*, 2004, **44**, 257–320.
22 F. Noack, *Prog. Nucl. Magn. Reson. Spectrosc.*, 1986, **18**, 171–276.
23 R. Y. Dong, *Nuclear Magnetic Resonance of Liquid Crystals*, Springer-Verlag, Berlin, 1997.
24 A. Abragam, *The Principles of Nuclear Magnetism*, Clarendon Press, Oxford, 1961.
25 R. Kimmich and H. W. Weber, *Phys. Rev. B: Condens. Matter Mater. Phys.*, 1993, **47**, 11788–11794.
26 M. Vilfan, T. Apih, P. J. Sebastiao, G. Lahajnar and S. Zumer, *Phys. Rev. E: Stat., Nonlinear, Soft Matter Phys.*, 2007, **76**, 051708.
27 N. Bloembergen, E. M. Purcell and R. V. Pound, *Phys. Rev.*, 1948, **73**, 679–712.
28 H. C. Torrey, *Phys. Rev.*, 1953, **92**, 962–969.
29 S. Zumer and M. Vilfan, *Phys. Rev. A: At., Mol., Opt. Phys.*, 1978, **17**, 424–433.
30 M. Vilfan and S. Zumer, *Phys. Rev. A: At., Mol., Opt. Phys.*, 1980, **21**, 672–680.
31 P. G. de Gennes and J. Prost, *The Physics of Liquid Crystals*, Clarendon Press, Oxford, 1993.
32 P. J. Sebastiao, D. Sousa, A. C. Ribeiro, M. Vilfan, G. Lahajnar, J. Seliger and S. Zumer, *Phys. Rev. E: Stat., Nonlinear, Soft Matter Phys.*, 2005, **72**, 061702.
33 S. Stapf, R. Kimmich and J. Neiss, *J. Appl. Phys.*, 1994, **75**, 529–537.
34 T. Zavada and R. Kimmich, *J. Chem. Phys.*, 1998, **109**, 6929–6939.
35 W. H. Press, B. P. Flennery, S. A. Teukolsky and W. T. Vetterling, *Numerical Recipes – the Art of Scientific Computation*, Cambridge University Press, Cambridge, 1986.
36 J. O. Mager, PhD thesis, University of Stuttgart, 1993.
37 M. Cifelli, P. J. McDonald and C. A. Veracini, *Phys. Chem. Chem. Phys.*, 2004, **6**, 4701–4706.
38 N. Leon, J. P. Korb, I. Bonalde and P. Levitz, *Phys. Rev. Lett.*, 2004, **92**, 195504.
39 A. Carvalho, P. J. Sebastiao, A. C. Ribeiro, H. T. Nguyen and M. Vilfan, *J. Chem. Phys.*, 2001, **115**, 10484–10492.
40 R. H. Acosta and D. J. Pusiol, *Phys. Rev. E: Stat. Phys., Plasmas, Fluids, Relat. Interdiscip. Top.*, 1999, **60**, 1808–1811.